RAA 2021 Vol. **21** No. **3**, 72(12pp) doi: 10.1088/1674-4527/21/3/72

http://www.raa-journal.org *http://iopscience.iop.org/raa*

***R**esearch in*
***A**stronomy and*
***A**strophysics*

GRB 130310A: very high peak energy and thermal emission

Song-Mei Qin[1,2], Lu-Yao Jiang[2,3], and Xiang-Gao Wang[2,3]

[1] Mathematics and Physics Section, Guangxi University of Chinese Medicine, Nanning 530001, China
[2] Guangxi Key Laboratory for Relativistic Astrophysics, the Department of Physics, Guangxi University, Nanning 530004, China; *wangxg@gxu.edu.cn*
[3] GXU-NAOC Center for Astrophysics and Space Sciences, School of Physical Science and Technology, Guangxi University, Nanning 530004, China

Received 2020 June 29; accepted 2020 September 14

Abstract The special GRB 130310A was observed by *Fermi* Gamma-Ray Burst Monitor and Large Area Telescope, with $T_{90} \sim 2.4$ s. With a combination of a Band function and a blackbody (BB) function, the time-resolved spectral analysis of GRB 130310A confirmed that there is a sub-dominate thermal component in the early period (e.g., slice $T_0 + [4.03 - 4.14]$ s) spectrum with BB temperature (kT) being $\sim 7 \sim 5$ keV, which can be interpreted as photosphere emission. The precursor of GRB 130310A can be fitted well with a BB component with $kT \sim 45$ keV, which is higher than that of the main burst. It suggests that the radiation of GRB 130310A is in transition from thermal to non-thermal. Such a transition is an indication of the change in jet composition from a fireball to a Poynting-flux-dominated jet. A very high peak energy is obtained in the first time bin, with the peak energy E_p of the Band component for Band+BB and Band model being $\sim 8.5 \sim 5.2$ MeV and $\sim 11.1 \sim 7.4$ MeV, respectively. Afterwards, the E_p drops to ~ 1 MeV. The E_p evolution patterns with respect to the pulses in the GRB 130310A light curves show a hard-to-soft evolution. The interpretation of the high peak energy E_p within the photosphere and internal shock model is difficult. It also suggests that at least for some bursts, the Band component must invoke a non-thermal origin in the optically thin region of a GRB outflow. Assuming the redshift is $z \sim 0.1 \sim 8$, the radius of the jet base $r_0 \sim 10^9$ cm to allow $(1 + \sigma_{15}) > 1$ in line with the calculation results of the magnetization parameter at $\sim 10^{15}$ cm (σ_{15}). However, the value of $(1 + \sigma_{15})$ is $\simeq 1$ in the zone z around 3 for $r_0 \sim 10^9$ cm, suggesting the non-excluded possibility that the origin is from ICMART with a low value. The photosphere-internal shock seems capable of interpreting the high peak energy, which requires electron Lorentz factor $\gamma_e \sim 60$ and $\epsilon_e \sim 0.06$.

Key words: gamma rays bursts: general — gamma-ray burst: individual (GRB 130310A) — radiation mechanisms: thermal — radiation mechanisms: non-thermal

1 INTRODUCTION

Gamma-ray bursts (GRBs) are the most powerful electromagnetic explosions in the Universe (e.g., Kumar & Zhang 2015; Zhang 2018). Multi-wavelength observations reveal at least two types of GRBs, among which one has typical long durations, believed to be deaths of some special massive stars (e.g., Narayan et al. 1992; Woosley 1993; MacFadyen & Woosley 1999; Berger et al. 2005; Tanvir et al. 2005; Fruchter et al. 2006; Zhang 2006) and the other one has typical short durations, associated with compact objects such as neutrons stars and black holes (e.g., Paczynski 1986; Eichler et al. 1989; Paczynski 1991; Abbott et al. 2017). According to the standard model, the broadband afterglow stems from the external shock as the fireball is decelerated by the ambient medium (e.g., Mészáros & Rees 1997; Sari et al. 1998; Wang et al. 2015), and the prompt gamma-ray emission is due to some internal dissipation processes.

The origin of GRB prompt emission is still not fully understood after more than 40 years of observations and remains an open question. Many GRB prompt emission models have been discussed, e.g., fireball internal shock model (e.g., Rees & Meszaros 1994; Kobayashi et al. 1997; Mészáros & Rees 2000; Daigne & Mochkovitch

1998), magnetized engine-internal shock model (e.g., Bošnjak et al. 2009; Zhang & Pe'er 2009; Daigne et al. 2011; Hascoët et al. 2013), dissipative photosphere model (e.g., Thompson 1994; Ghisellini et al. 2007; Rees & Mészáros 2005; Giannios 2008; Beloborodov 2010; Ioka 2010; Lazzati et al. 2010; Veres et al. 2012; Bégué & Pe'er 2015), and internal collision-induced magnetic reconnection and turbulence (ICMART) model (Zhang & Yan 2011). In addition, quasi-thermal (blackbody (BB) component) and non-thermal component emission have been predicted by models in spectra of GRBs (e.g., Mészáros & Rees 2000; Zhang & Mészáros 2002; Daigne & Mochkovitch 2002; Ramirez-Ruiz et al. 2002; Pe'er et al. 2006; Ghisellini et al. 2007; Pe'er et al. 2012; Toma et al. 2011; Zhang & Yan 2011; Piro et al. 2014; Nakar & Piran 2017; Pe'er & Ryde 2017). The comprehensive prompt emission has shown that the spectrum may include three components, e.g., the non-thermal "Band" component, the quasi-thermal component and the non-thermal component, which can be fit as a power law extending to high energies (Zhang et al. 2011). Most observational spectra are fitted well by an empirical function of two smoothly connected power laws, which is the so-called "Band" function (Band et al. 1993), with a typical value of the lower energy photon spectral index of $\alpha \sim -1 \pm 1$ and the typical value of observed E_p is 200–300 keV (e.g, Preece et al. 2000; Zhang et al. 2011; Nava et al. 2011; Goldstein et al. 2012; Bosnjak et al. 2013; Gruber et al. 2014). There also exist some observed low-energy power-law indices of the Band component, which are found to be harder than the synchrotron death line (α =-2/3) (e.g., Preece et al. 1998; Sari et al. 1998). The (quasi-)thermal component (photosphere component) is found to contribute to the observed spectra of GRBs. The thermal component can dominate the spectrum in rare cases such as GRB 090902B (Ryde et al. 2010; Zhang & Yan 2011), GRB 081221 (Hou et al. 2018), GRB 100507 (Ghirlanda et al. 2013), GRB 101219B (Larsson et al. 2015) and GRB 160625B (the first episode of prompt emission) (Lü et al. 2017; Zhang et al. 2018). Some GRBs show up as a superposed bump in the low-energy wing of the Band function such as GRB 100724B (Guiriec et al. 2011), GRB 110721A (Axelsson et al. 2012; Zhang et al. 2012), GRB 120323A (Guiriec et al. 2013) and GRB 141207A (Arimoto et al. 2016). Most GRBs exhibit a phenomenon such that their thermal components are essentially suppressed, e.g., spectra of GRB 080916C can be described well by the Band function in five different time bins over $6-7$ orders of magnitude in energy (Abdo et al. 2009; Zhang & Yan 2011).

In view of the fact that the broadening mechanism incorporates both physical broadening (Compton upscattering of the seed thermal photons) and geometric broadening (the effect of equal-arrival-time volume), the Band function itself is argued to possibly be emission from a dissipative photosphere (e.g., Rees & Mészáros 2005; Giannios 2008; Pe'er 2008; Giannios 2012; Beloborodov 2010; Ioka 2010; Lazzati & Begelman 2010; Pe'er & Ryde 2011; Vurm et al. 2011; Lundman et al. 2013; Bégué & Pe'er 2015; Meng et al. 2018; Liu et al. 2018; Parsotan et al. 2018; Ryde et al. 2019; Bhattacharya & Kumar 2020). This model purports that photosphere emission has a high efficiency and the photosphere temperature could reach above MeV, which is in the range of the observed E_p distribution. The photosphere model has also been argued to be able to interpret the *Amati* relation and other correlations (e.g., Amati et al. 2002; Fan et al. 2012; Giannios 2012; Ito et al. 2019). There is one case in which *Fermi* observations of GRB 110721A have revealed an unusually high peak energy $E_p \sim 15$ MeV at the early epochs that exceeds the "death line" of the photosphere emission (Zhang et al. 2012), signifying that the thermal origin of E_p is ruled out in this burst, since it exceeds the maximum temperature for a non-dissipative photosphere to reach the observed luminosity (Zhang et al. 2012; Veres et al. 2012). The question of whether the dominant radiation mechanism is quasi-thermal or non-thermal remains a debate in the GRB community (e.g., Zhang 2014), which is also relevant to the origin of the "Band" spectral component observed in most GRBs, the dominant spectral component of GRB prompt emission. The corresponding answer is of great importance to research on other open questions in the physics of GRBs, e.g., central engine, jet composition and energy dissipation mechanisms (e.g., Zhang 2011, 2015; Pe'er 2015; Dai, Daigne & Mészáros 2017).

A special *Fermi* GRB 130310A is a case that is similar to GRB 110721A, with a very high peak energy E_p of the Band function and a sub-dominate thermal component in the early period spectrum. In this paper, we present an analysis of a special GRB 130310A. Details on data reduction of the *Fermi* observation, as well the analysis of time-integrated and time-resolved spectra, are described in Section 2. The thermal emission of GRB 130310A is presented in Section 3. The very high E_p and its possible physical interpretations are reported on in Section 4. The conclusion and discussion are provided in Section 5. Throughout the paper, a concordance cosmology with parameters $H_0 = 71\,\mathrm{km\ s^{-1}\ Mpc^{-1}}$, $\Omega_M = 0.30$ and $\Omega_\Lambda = 0.70$ is considered. $F \propto t^\alpha \nu^\beta$ is adopted. Moreover, the convention $Q = 10^n Q_n$ is adopted for cgs units.

2 OBSERVATIONS AND ANALYSIS

2.1 Observations and Data Reduction

GRB 130310A was triggered (trigger 384638984/130310840) by *Fermi*/Gamma-Ray Burst Monitor (GBM) on 2013 March 10 at 20:09:41.50 UT (defined as T_0; UT dates are used throughout this paper) with $T_{90} \sim 2.4$ s (50-300 keV) (Xiong & Chaplin 2013). It was detected by *Fermi*/Large Area Telescope (LAT) on 2013 March 10 at 20:09:44 UT, about 3 s after the *Fermi*/GBM trigger time (Guiriec et al. 2013). Also, GRB 130310A was observed by *Konus-Wind* (Golenetskii et al. 2013), *Suzaku*/WAM (Kawano et al. 2013), *INTEGRAL*/SPI-ACS, *MESSENGER*/GRNS and *Mars Odyssey*/HEND (Golenetskii et al. 2013), with no certain *Swift*/XRT or optical candidate detected (Sbarufatti et al. 2013; Butler et al. 2013; Cucchiara et al. 2013).

We downloaded the GBM and LAT data of GRB 130310A from the public science support center at the official *Fermi* website[1]. GBM has 12 sodium iodide (NaI) scintillation detectors covering energy from 8 keV to 800 keV, and two bismuth germanate (BGO) scintillation detectors sensitive to higher energies between 200 keV and 40 MeV (Meegan et al. 2009). There are three different types of signals from *Fermi*/GBM detectors, CTIME, CSPEC and TTE[2]. We extract the time-integrated and time-resolved spectra from the TTE data files. The background spectra of the GBM data are extracted from the CSPEC format data with user-defined intervals before and after the prompt emission phase. Two types of LAT data are available, the LAT Low-Energy (LLE) data in the 20 MeV−1 GeV band and the high-energy LAT data in the 100 MeV−300 GeV band, which were reduced utilizing the *gtBurst*[3] package and the P8TRANSIENT 020E response function. The event energy flux (8–1000 keV) from *Fermi*/GBM is $1.02\pm0.21\times10^{-5}$ erg cm^{-2} s^{-1} in the time-integrated spectrum. With the *gtBurst* package, we perform spectral analysis using data from the NaI_9, NaI_a and BGO 1 detectors. Also, the LLE data are included. As displayed in Figure 1, the light curves of GRB 130310A consist of two pulses and a precursor (Xiong & Chaplin 2013).

[1] ftp://legacy.gsfc.nasa.gov/fermi/data/

[2] The continuous time (CTIME) data include eight energy channels and have a finer time resolution of 64 ms. The continuous spectroscopy (CSPEC) data include 128 energy channels, and a time resolution of 1.024 s. The time-tagged event (TTE) data consist of individual detector events, each tagged with arrival time, energy (128 channels) and detector number.

[3] http://sourceforge.net/projects/gtburst/

2.2 Spectral Analysis

We firstly employed the typical empirical Band function to fit *Fermi* data of GRB 130310A. The Band function (Band et al. 1993) is described as a smoothly broken power law,

$$N_{\rm Band}(E) = A_1 \begin{cases} (\frac{E}{100\ {\rm keV}})^{\alpha}\exp(-\frac{\rm E}{\rm E_0}), \\ (E < (\alpha-\beta)E_0) \\ [\frac{(\alpha-\beta)E_0}{100\ {\rm keV}}]^{\alpha-\beta}\exp(\beta-\alpha)(\frac{\rm E}{100\ {\rm keV}})^{\beta}, \\ (E \geq (\alpha-\beta)E_0) \end{cases} \quad (1)$$

where A_1 is the normalization of the Band spectrum, α and β are the low- and high-energy photon spectral indices, respectively; E is the observational photon energy; E_0 is the break energy of the spectrum; the peak energy (E_p) of the spectrum is related to E_0 through $E_p = (2+\alpha)E_0$. The above fitting results of GRB 130310A are listed in Table 1. The time-integrated spectrum ($T_0+[4.03-5.0]$ s) can be fitted with the Band function, with $E_p = 2446.2 \pm 226.6$ keV, $\alpha = -1.03 \pm 0.01$, $\beta = -2.58 \pm 0.09$ and $PGSTAT/dof = 454/391$ (as plotted in Fig. 2). To investigate the properties of time-resolved spectra, we divided the spectrum into four slices, e.g., Slice a ($T_0 + [4.03 - 4.14]$ s), Slice b ($T_0 + [4.14 - 4.23]$ s), Slice c ($T_0 + [4.23 - 4.45]$ s) and Slice d ($T_0 + [4.45 - 5.00]$ s). The time-resolved spectra are guaranteed to have a signal-to-noise ratio (SNR) >35 in each time-bin. The analysis of time-resolved spectral results shows a noticeable feature in GRB 130310A in that a considerably high peak energy $E_p = 9265.0\pm1380.4$ keV is obtained in Slice a, with $\alpha = -1.15 \pm 0.02$, $\beta = -3.69 \pm 2.77$ and $PGSTAT/dof = 434/391$. Then, E_p declines very fast, with the values of $E_p = 1656.2 \pm 257.8$ and 888.1 ± 133.1 keV for Slices b and c, respectively. For the second pulse (Slice d), the peak energy is $E_p = 1076.3 \pm 272.4$ keV, with $\alpha = -1.03 \pm 0.01$, $\beta = -2.84 \pm 0.67$ and $PGSTAT/dof = 393/346$.

A thermal component is invoked to describe the fireball photosphere emission (e.g., Rees & Mészáros 2005; Giannios 2008; Beloborodov 2010). A sub-dominate thermal component has been found in some cases, e.g., GRB 110721A, 100724B and 120323A. Besides, we also try to test if there is thermal emission for the GRB 130310A, with a Band function plus a BB function (Band + BB). The BB function can be described as,

$$N_{\rm BB}(E) = \frac{A_2 \times 8.0525E^2dE}{(kT)^4(e^{(E/kT)}-1)}, \quad (2)$$

where A_2 is the normalization of the BB spectrum and kT is the BB temperature. The Band + BB has more free parameters than the Band model. A tool for model selection (e.g., Kass & Raftery 1995; Wei et al. 2016; Lü et al. 2017; Zhang et al. 2018), Bayesian Information

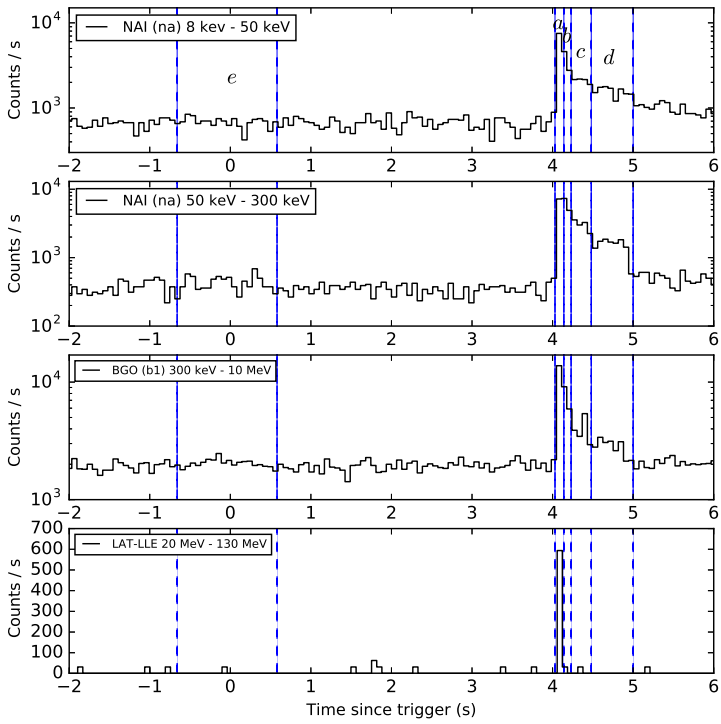

Fig. 1 GBM light curves for the gamma-ray emission of GRB 130310A. Light curves from different energy ranges are presented in different panels. The main light curves are divided into four slices for time-resolved spectral analysis, e.g., Slice a ($T_0 + [4.03 - 4.14]$ s), Slice b ($T_0 + [4.14 - 4.23]$ s), Slice c ($T_0 + [4.23 - 4.45]$ s) and Slice d ($T_0 + [4.45 - 5.0]$ s). The precursor is also marked as Slice e.

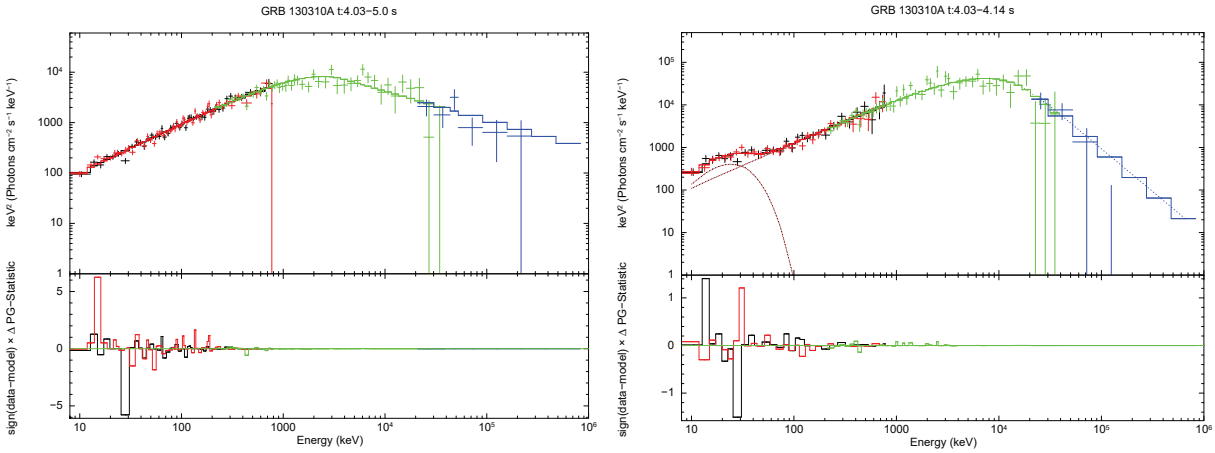

Fig. 2 Spectral fitting of GRB 130310A. *Left panel*: Time-integrated spectral fitting with Band function; *Right panel*: Time-resolved spectral fitting with Band+BB function for Slice a.

Criterion (BIC), prefers the model with the lowest BIC value. If $\Delta\mathrm{BIC} = 2 - 6$ (ΔBIC=BIC$_1$-BIC$_2$, where subscripts represent different models), it signifies positive evidence of improvement in model 2; if $\Delta\mathrm{BIC} = 6 - 10$, it points to strong evidence for model 2; if $\Delta\mathrm{BIC} > 10$, it represents very strong evidence for model 2. The results are displayed in Table 1. By comparing their BIC, we found that Slice a can be fitted well with the Band+BB model (as depicted in Fig. 2 and Fig. 3), with $\Delta\mathrm{BIC} = 53$. In this slice, a relatively lower kT value is 6.2 ± 0.5 keV and a high Band peak energy value is 7376.2 ± 947.8 keV. The results of ΔBIC for other slices and time-integrated spectra suggest that the Band model is more favored. There are no obvious spectral lags found in GRB 130310A.

Table 1 GRB 130310A Spectral Fitting with Band Model and Band+BB Model

Time interval	Band			$PGSTAT/dof$	Band+BB				$PGSTAT/dof$	AIC_{B-Bbb}	BIC_{B-Bbb}
(s)	α	β	E_{p} (keV)		α	β	E_{p} (keV)	kT(keV)			
(1)	(2)	(3)	(4)	(5)	(6)	(7)	(8)	(9)	(10)	(11)	(12)
$[-0.66-0.58]$	-0.22	-1.73±0.33	220.8±341.8	412/346	...	...	...	45.4±7.0	418/348		7.1
$[4.03-4.12]$	-1.24±0.03	-8.00	9310.8±2262.7	386/391	-1.02±0.06	-4.21±2.32	7132.7±1586.4	7.1±0.8	363/389	18.8	10.8
$[4.12-4.13]$	-1.10±0.03	-5.00	11121.6±2605.1	411/391	-0.87±0.06	-4.41±2.40	8499.4±1695.4	6.0±0.8	382/389	24.9	16.9
$[4.13-4.14]$	-1.02±0.04	-4.44	7403.0±1422.1	357/391	-0.80±0.08	-3.14±0.60	5168.9±1383.1	5.0±1.0	341/389	12.5	4.6
$[4.03-4.14]$	-1.15±0.02	-3.69±2.77	9265.0±1380.4	434/391	-0.94±0.04	-4.01±0.96	7376.2±947.8	6.2±0.5	369/389	60.9	52.9
$[4.14-4.23]$	-0.84±0.04	-2.34±0.09	1656.2±257.8	367/391	-0.76±0.06	-2.29±0.08	1418.7±269.2	3.2±1.4	362/389	0.9	-7.0
$[4.23-4.45]$	-0.73±0.05	-2.54±0.15	888.1±133.1	434/391	-0.82±0.07	-2.64±0.19	1193.4±327.4	54.6±14.7	430/389	-0.8	-8.7
$[4.45-5.0]$	-1.03±0.05	-2.84±0.67	1076.3±272.4	398/346	-0.98±0.09	-2.79±0.63	990.3±331.4	4.1±3.6	398/344	-3.4	-11.2
$[4.03-5.0]$	-1.03±0.01	-2.58±0.09	2446.2±226.6	454/391	-1.05±0.03	-2.60±0.10	2636.5±4.0	1.2±35.5	450/ 389	0.5	-7.5

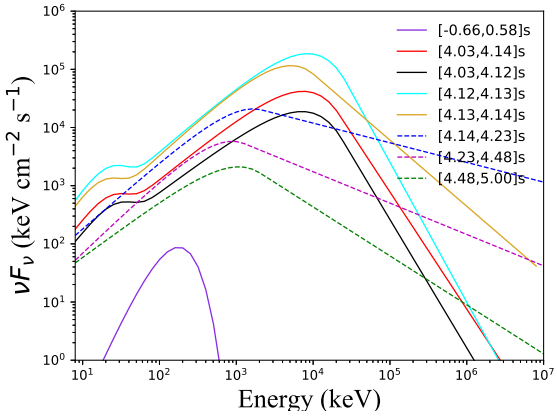

Fig. 3 Best-fit νF_ν model spectra for the time-resolved data in different time bins (as marked in the legend).

Since the spectral evolution is initially very rapid in Slice a, we adjust the SNR > 20 to provide higher temporal resolution time bins, to further investigate the evolution of the Band/BB component. As the burst is very bright, we can divide the first time bin (Slice a) into three. The results (as listed in Table 1) affirm that there also exist features of very high $E_p \sim 11.1$ MeV and a sub-dominate thermal component. The peak energy E_p of the Band component for the Band+BB and Band model is $\sim 8.5 \sim 5.2$ MeV and $\sim 11.1 \sim 7.4$ MeV. The kT value varies from 7.1 to 5.0 keV.

Furthermore, we also try to do the spectral fitting of the precursor of GRB 130310A (Slice e in Fig. 1). The best fitting parameters of the Band function model are $\alpha = -0.22$ and $\beta = -1.73 \pm 0.33$ with $PGSTAT/dof = 412/346$. Our results show that the α of the precursor of GRB 190109A is significantly harder than the typical value $\alpha \sim -1$ (e.g, Preece et al. 2000; Zhang & Yan 2011; Nava et al. 2011; Bosnjak et al. 2013). The α value of Slice e is also harder than those predicted by the synchrotron regime of the fast cooling case ($\alpha = -3/2$) and the slow cooling case ($\alpha = -2/3$, also called the synchrotron line of death) (e.g., Preece et al. 1998). According to some GRBs (e.g., GRB 090902B), the related spectral width is found to be very narrow, suggesting the probable existence of a quasi-thermal component. Then we also fit the precursor with a BB function. The best fitting parameters of the BB model are $kT = 45.4 \pm 7.0$ keV and $PGSTAT/dof = 418/348$. Comparing the BIC between Band and BB model, we found that the BB model is stronger than the Band model in Slice e, with $\Delta\mathrm{BIC} = 7.1$ (as displayed in Fig. 4 and Table 1).

3 THE THERMAL EMISSION IN GRB 130310A

The results of spectral analysis indicate the existence of thermal emission during the early period, e.g., Slice a. Compared with BIC, Akaike Information Criterion (AIC) (Akaike 1974) is relatively looser and can also be applied in astronomy (e.g., Burnham & Anderson 2002; Liddle 2004, 2007; Tan & Biswas 2012; Wei et al. 2013; Melia & Maier 2013). If AIC is utilized to compare the fitting results between the Band and Band+BB models, thermal emission seems to be not completely ruled out in Slice b, with BB temperature $kT \sim 3$ keV. Possibly, the reasons lie in that the thermal emission is weak and the BB temperature is lower, which cannot satisfy the BIC. Although AIC is not as strict as BIC, results from AIC can be employed to explore the physical properties of the GRB photosphere. It is interesting that the precursor can be fitted well by a pure BB model, with a higher kT value than those of the main burst. It suggests that the radiation of GRB 130310A is in transition from thermal to non-thermal. In the precursor, the pure BB component suggests that the jet composition has a hot fireball origin. In the main burst, it consists of a sub-dominant thermal component and a dominant synchrotron component (Poynting-flux-dominated), suggesting a likely hybrid jet composition. Such a transition is an indication of the change in jet composition from a fireball to a Poynting-flux-dominated jet.

The jet composition of GRBs is suggested to be diverse (e.g., Zhang & Yan 2011; Gao & Zhang 2015), for the various spectral behaviors of GRB prompt emission may be concerned with disparate σ_0 values at the central

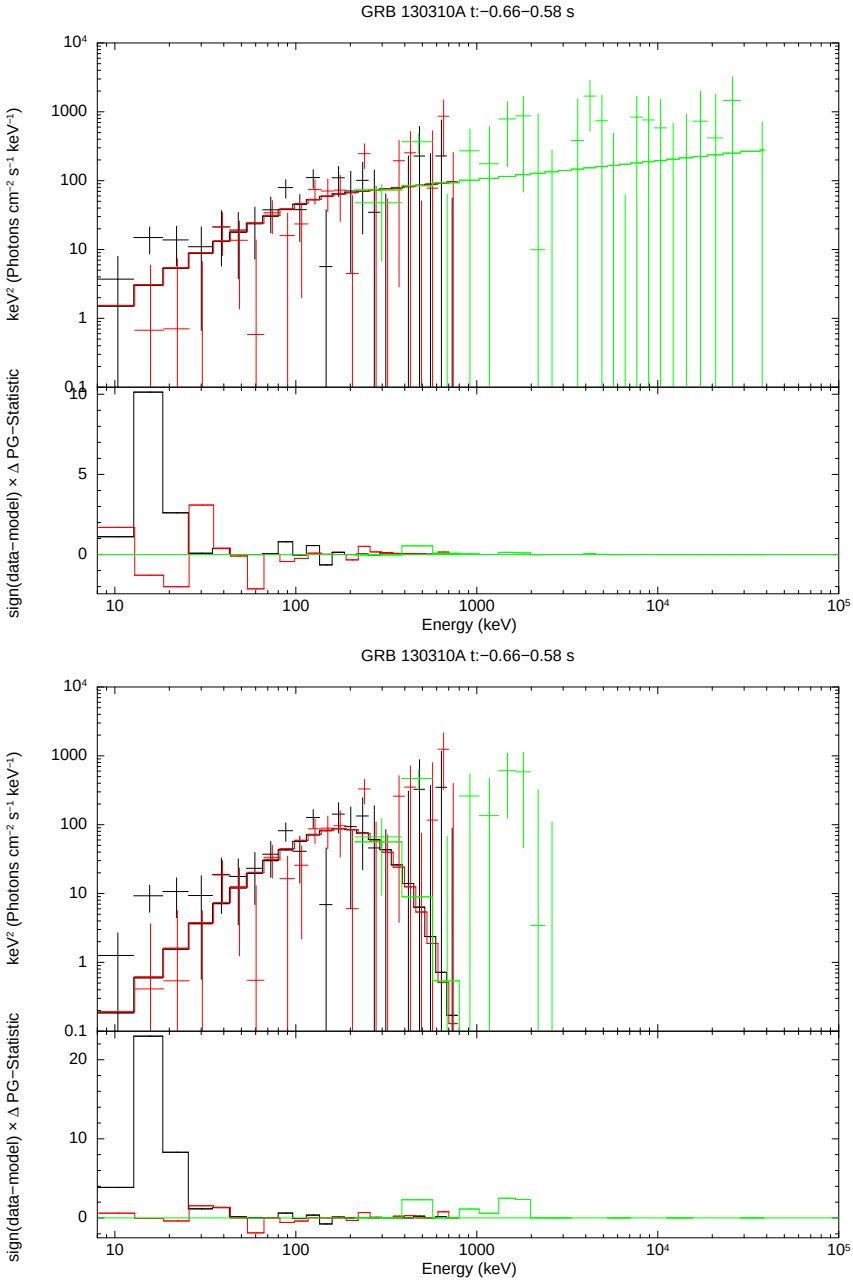

Fig. 4 Spectral fitting of GRB 130310A precursor (Slice e). *Upper panel*: Spectral fitting with Band function; *Lower panel*: Spectral fitting with BB function.

engine, where σ_0 represents the ratio between Poynting flux and matter flux at the central engine. There are three types: the first one is very small σ_0 ($\sigma_0 \ll 1$), with the observed spectrum dominated by the photosphere emission component (e.g. in GRB 090902B); the second one is moderately high σ_0, with the suppressed thermal emission of sub-dominant photosphere emission component in the observed spectrum (e.g., in GRB 110721A, GRB 120323A); the last one has extremely high σ_0, with the completely suppressed photosphere component, and the observed spectrum dominated by the non-thermal Band component. GRB 130310A is similar to GRB 110721A, which has been suggested to belong to the second type. Following a hybrid photosphere emission model of Gao & Zhang (2015), we derive the parameters of the photosphere, e.g., the radius of the photosphere $r_{\rm ph}$, the Lorentz factor of the photosphere $\Gamma_{\rm ph}$, the magnetization parameter at the photosphere $\sigma_{\rm ph}$, as well as the dimensionless entropy of hot fireball component η and σ_0. Assuming the radius of the jet base is $r_0 \sim 10^7 \sim 10^9$ cm and redshift is $z \sim 0.1 \sim 8$, the calculation results of GRB 130310A are depicted in Figures 5–7. For $r_0 \sim 10^7$

cm in the first time bin, the value of $(1+\sigma_0)$ is [1.2, 8.7]; the value of η is [11.4, 778.6]; the value of $r_{\rm ph}$ is $[3.13\times10^{12}, 1.22\times10^{14}]$ cm; the value of $\Gamma_{\rm ph}$ is [118.8, 1246.7]; the value of $(1+\sigma_{\rm ph})\sim1$. Concerning $r_0\sim10^8$ cm in the first time bin, the value of $(1+\sigma_0)$ is [5.4, 40.5]; the value of η is [2.5, 167.8]; the value of $r_{\rm ph}$ is $[3.13\times10^{12}, 1.22\times10^{14}]$ cm; the value of $\Gamma_{\rm ph}$ is [97.7, 1246.7]; the value of $(1+\sigma_{\rm ph})\sim1$. For $r_0\sim10^9$ cm in the first time bin, the value of $(1+\sigma_0)$ is [25.0, 96.8]; the value of η is [3.1, 103.8]; the value of $r_{\rm ph}$ is $[1.65\times10^{12}, 7.04\times10^{13}]$ cm; the value of $\Gamma_{\rm ph}$ is [54.9, 877.0]; the value of $(1+\sigma_{\rm ph})$ is [3.3, 14.1]. As mentioned in this section, while AIC is less strict than BIC, results from the former can be used to probe the physical properties of the GRB photosphere, suggesting that a thermal component could not be ruled out in the second time bin as well. The derived $(1+\sigma_0)$ increases with time from the first to the second time bin, which is consistent with the expectation of some central engine models (e.g., Metzger et al. 2011; Gao & Zhang 2015; Lei et al. 2017). For photosphere emission in the precursor, concerning $r_0\sim10^7$ cm, the values of η, $r_{\rm ph}$ and $\Gamma_{\rm ph}$ are [211.9, 3662.2], $[1.64\times10^{10}, 4.65\times10^{11}]$ cm and [69.5, 729.4], respectively.

4 THE VERY HIGH PEAK ENERGY IN GRB 130310A AND POSSIBLE PHYSICAL IMPLICATION

As was mentioned in Section 2.2, the very high peak energy is obtained in the first time bin (Slice a, $T_0+[4.03-4.14]$ s). Here the peak energy of the Band component for Band+BB and Band model is $\sim 8.5\sim5.2$ MeV and $\sim 11.1\sim7.4$ MeV, respectively. After the first time bin, the E_p drops to ~1 MeV. In regards to E_p evolution patterns with respect to the pulses in the light curves, they seem to show hard-to-soft evolution and intensity tracking in the first pulse ($T_0+[4.03-4.45]$ s) and the second pulse ($T_0+[4.45-5.0]$ s), respectively (as depicted in Fig. 8). Previous research suggests that the E_p evolution behavior of the second pulse with intensity-tracking may be generated by the superposition of two hard-to-soft pulses (Lu et al. 2012; Hakkila & Preece 2011). We also present the best-fit νF_ν model curves in different time intervals in Figure 3. The evolution of the spectral shape of the Band component shows a similar α value to that of gradually shallowing β, which reflects extremely high similarity with the result from Lu et al. (2012) in that the higher E_p may be the superimposed spectrum. This demonstrated that the E_p evolution patterns are dominated by hard-to-soft evolution in the global light curves of GRB 130310A, and the Band component should share an identical physical origin in different epochs.

We try to test the high peak energy E_p in disparate GRB models, e.g., non-photosphere, dissipative photosphere, ICMART, internal shock and photosphere-internal shock.

- We first assume that a GRB spectrum is dominated by the photosphere emission. For a certain observed isotropic gamma-ray luminosity $L=L_{ph}$ (L_{ph} is photosphere luminosity), the E_p could not exceed the death line of baryonic photosphere emission, which could be defined as $E_p\leq\zeta kT_0\simeq1.2\,{\rm MeV}\,\zeta L_{52}^{1/4}r_{0,7}^{-1/2}$, with ζ being a factor that denotes the νF_ν peak of the photosphere spectrum (Zhang et al. 2012). Figure 9 features the rest-frame E_p-L plot for time-resolved spectra of GRB 130310A with summing redshift $z\sim0.1\sim8$. Furthermore, the special GRB 110721A with a very high peak energy (~15 MeV) and a sub-sample of Lu et al. (2012) is also presented together there. Two death lines that correspond to $r_0\sim10^7$ cm (typical value) and $r_0\sim3\times10^6$ cm (extreme value to allow the highest possible death line) are drawn. According to Figure 9, the unusually observed very high E_p of GRB 130310A in the first time bin is close to the maximum temperature allowed by the non-saturated dissipative photosphere model.
- A dissipative photosphere has been employed to explain the very high peak energy E_p of GRB 110721A (Veres et al. 2012). The magnetic dissipative photosphere model predicts a high E_p $\sim$8 MeV (Bégué & Pe'er 2015). Compared with GRB 110721A, the very high E_p of GRB 130310A is found together with a thermal component supposed to be the photosphere origin in the first time bin. Then, the primary Band component must be another component. Since the Band component extends below the thermal component, it must not be self-absorbed in the emission region, which means this component comes from an optically-thin region far above the photosphere (Zhang 2014). Furthermore, the very rapid hard-to-soft E_p evolution of GRB 130310A is also a challenge to the photosphere model (e.g., Zhang & Yan 2011). Therefore, the very high energy E_p of GRB 130310A is likely to stem from an optically thin region with accelerated non-thermal particles.
- Within the ICMART model, the hard-to-soft E_p evolution is naturally expected, since one pulse corresponds to one radiation unit and magnetic field

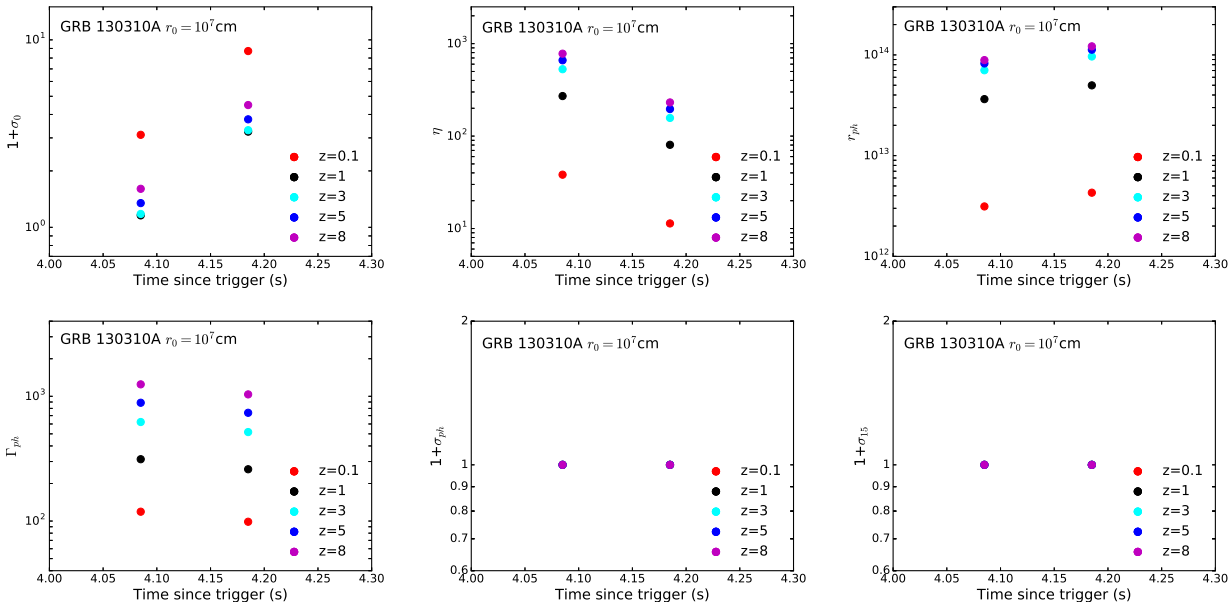

Fig. 5 The calculation results of photosphere parameter for GRB 130310A, including the magnetization at the central engine σ_0; (b) the dimensionless η, the radius of the photosphere $r_{\rm ph}$, the Lorentz factor of the photosphere $\Gamma_{\rm ph}$, the magnetization parameter at the photosphere $\sigma_{\rm ph}$ and the magnetization parameter at $\sim 10^{15}$ cm σ_{15}. Here, we assume the size of the jet base $r_0 \sim 10^7$ cm and redshift $z \sim 0.1 \sim 8$ (as marked in the legend).

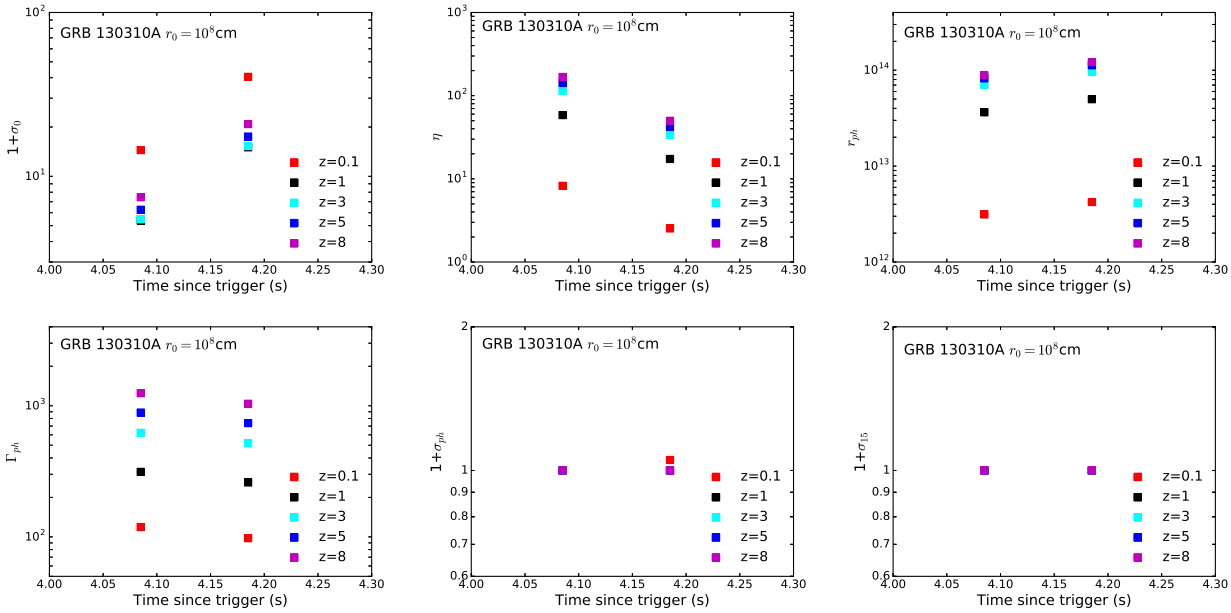

Fig. 6 The same as Fig. 5, but for $r_0 \sim 10^8$ cm.

strength falls as the emitter expands (Uhm & Zhang 2014; Zhang 2018). To check whether ICMART is responsible for the non-thermal emission, we also derive the magnetization parameter at $\sim 10^{15}$ cm. If the $\sigma_{15} \ll 1$ ($(1+\sigma_{15}) \simeq 1$), it means that 10^{15} cm is already in the coasting regime, and thus internal shock should be the key mechanism for non-thermal energy dissipation (Daigne et al. 2011). If the $(1+\sigma_{15}) > 1$, significant non-thermal emission is suggested to be generated through ICMART (Zhang & Yan 2011). The results (as displayed in Figs. 5–7(f)) show the value of $(1+\sigma_{15}) \simeq 1$ for $r_0 = 10^7$ and 10^8 cm, and that of $(1+\sigma_{15}) > 1$ for $r_0 = 10^9$ cm (noting that the $(1+\sigma_{15}) \simeq 1$ for $z \sim 3$). If the high peak energy E_p in the band component of GRB 130310A originates from the ICMART, it needs $r_0 \sim 10^9$ cm. However,

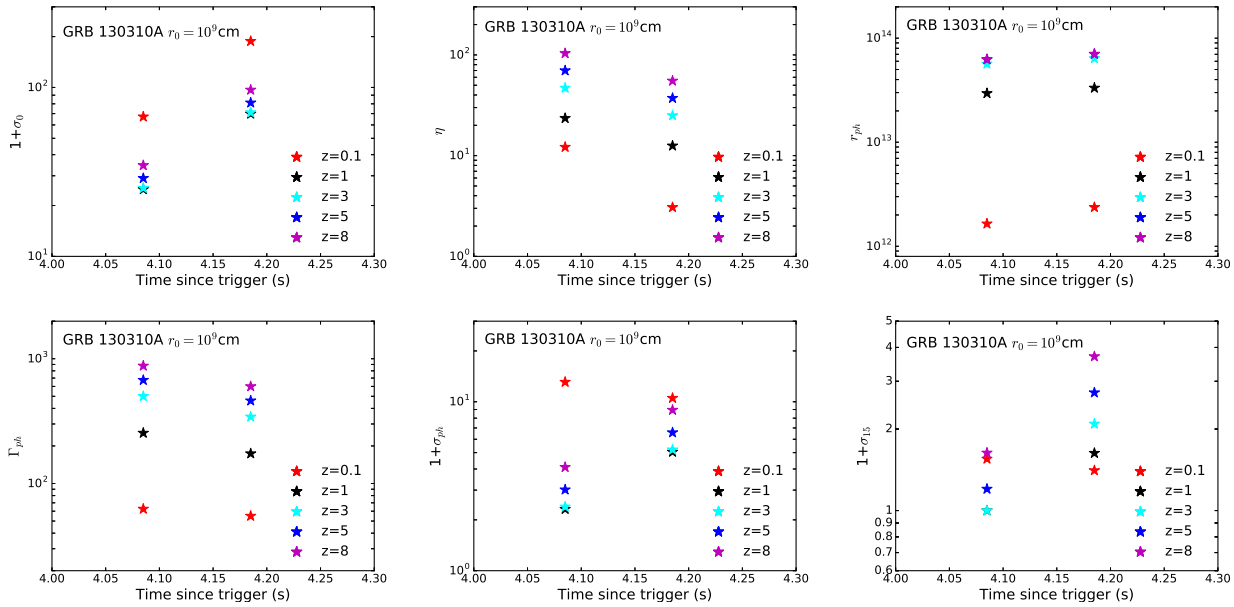

Fig. 7 The same as Fig. 5, but for $r_0 \sim 10^9$ cm.

the value of $(1 + \sigma_{15})$ is $\simeq 1$ in the zone z around 3 for $r_0 \sim 10^9$ cm, signifying a low possibility that the origin is from ICMART.

– It is supposed that the internal shock model can interpret the hard-to-soft E_p evolution in GRBs (e.g., Preece et al. 2014). For a low σ internal model, the peak energy could be defined as $E_p \simeq (200\,\mathrm{keV})\varepsilon_{x1}\varepsilon_{x2}^2 \sin\Psi (L_{52}^{1/2} r_{13}^{-1})(1+z)^{-1}$ (Zhang & Mészáros 2002), where $\varepsilon_{x1} = 0.82[\sigma/(1+\sigma)]^{1/2} + 1.4(\zeta_1 \epsilon_{B,-1}\theta_p)^{1/2}$; $\varepsilon_{x2} = [f(p)/(1/6)](\epsilon_e/\xi_e)\theta_p$; Ψ is the mean pitch angle of the electrons; ζ is the compressive ratio (at least 7 for strong shocks); $\theta_p = (\gamma_i/\gamma_j + \gamma_j/\gamma_i)/2 - 1)$; $f(p) = (p-2)/(p-1)$; r_i and r_j are the Lorentz factors of the two colliding shells; ξ_e is the injection fraction of the electrons; ϵ_e and ϵ_B are the fraction of shock energy to electron energy and magnetic field energy, respectively; p is the electron spectral index. Here the minimum Lorentz factor of the injected electrons $\gamma_e = f(p)(m_p/m_e)(\epsilon_e/\xi_e)\theta_p \simeq 310\varepsilon_{x2}$, where m_p and m_e are the mass of the proton and the electron, respectively. Thus, it is hard for the low σ internal shock model to explain the high energy E_p of GRB 130310A.

– In the model of photosphere-internal shock, the photospheric emission of the jet in GRBs can be Compton upscattered in the internal shocks (e.g., Toma et al. 2011). In this scenario, the peak photon energy of the Band function and photosphere emission has a relation of $E_p \sim E_{\rm ph}\gamma_e^2$. For this burst, $E_{\rm ph} \sim 24$ keV and $E_p = 7.4$ MeV can be required, with the electron Lorentz factor γ_e supposed to be around 60. Since $\gamma_e = f(p)(m_p/m_e)(\epsilon_e/\xi_e)\theta_p \simeq 310\varepsilon_{x2}$ (e.g., $\epsilon_e = 0.3$) (Zhang & Mészáros 2002), this requirement can be satisfied if $\epsilon_e \sim 0.06$ is adopted in the internal shock model.

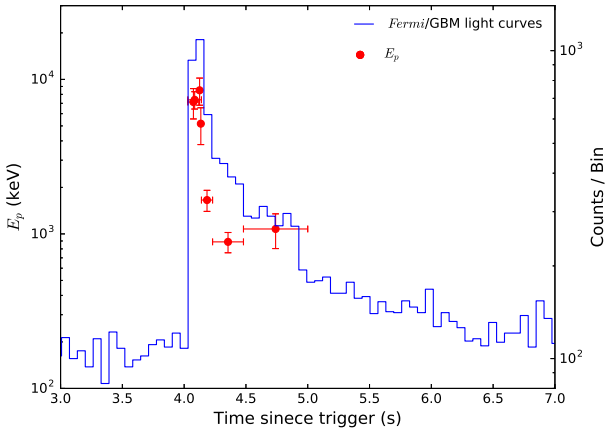

Fig. 8 Light curves (*blue lines*) presented along with the E_p evolution (*red circles with error bars*) of GRB 130310A.

5 CONCLUSIONS AND DISCUSSION

In this paper we have presented the time-integrated and time-resolved spectral analysis of the *Fermi* GRB 130310A. We arrive at the following interesting results:

1. The spectral analysis results of GRB 130310A suggest that there is a sub-dominate thermal component in

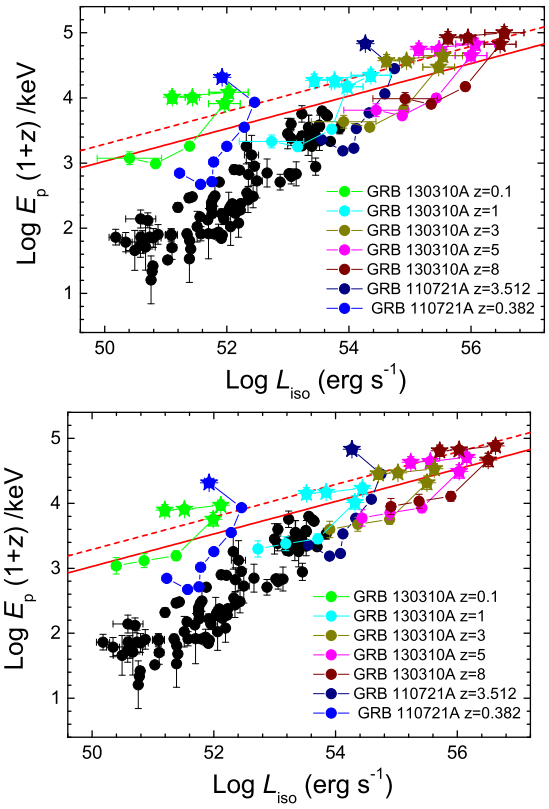

Fig. 9 Rest-frame peak energy $E_p(1+z)$ is plotted against the observed isotropic gamma-ray luminosity L. The data on GRB 130310A for different redshift are marked with different colors (as illustrated in the legend). The data of GRB 110721A (*blue points*) (Zhang et al. 2012) and sample of Lu et al. (2012) (*black points*) are also presented here. The stars are for the first epoch, which are all beyond the death lines. Two death lines are plotted, which correspond to $r_0 = 10^7$ cm (*solid*) and $r_0 = 3 \times 10^6$ cm (*dashed*), respectively. The upper and lower panels display the E_p and L from Band and Band+BB model, respectively.

the early period spectrum (the first time bin, Slice a, $T_0 + [4.03 - 4.14]$ s), with the derived BB temperature (kT) being $\sim 7 \sim 5$ keV. The precursor of GRB 130310A can be fitted well with a BB component with $kT = 45.4 \pm 7.0$ keV, which is higher than that of the main burst. It suggests that the radiation of GRB 130310A is in a transition from thermal to non-thermal. Such a transition is an indication of the change of jet composition from a fireball to a Poynting-flux-dominated jet.

2. In the first time bin (Slice a, $T_0 + [4.03 - 4.14]$ s), the very high peak energy is obtained, with the peak energy E_p of the Band component for Band+BB and Band model being $\sim 8.5 \sim 5.2$ MeV and $\sim 11.1 \sim 7.4$ MeV, respectively. Afterwards, the E_p drops to $\sim$ 1 MeV. E_p evolution patterns regarding the pulses in the GRB 130310A light curves exhibit the hard-to-soft evolutionary trend.

GRB 130310A and GRB 110721A are alike in that the photosphere emission component is sub-dominant in the observed spectrum, where the photosphere emission is related to the value of σ_0. Based on a hybrid photosphere emission model of Gao & Zhang (2015), we derive the parameters of the photosphere, e.g., σ_0, η, $r_{\rm ph}$, $\Gamma_{\rm ph}$ and $\sigma_{\rm ph}$. Assuming $r_0 \sim 10^7 \sim 10^9$ cm and redshift $z \sim 0.1 \sim 8$, we obtain a series of results that are consistent within the model that the thermal component is produced by the fireball when it becomes transparent.

To explain the high peak energy E_p, we test the high peak energy E_p in different GRB models, e.g., non-photosphere, dissipative photosphere, ICMART, internal shock and photosphere-internal shock. The $E_p - L$ plot indicates that the observed very high E_p of GRB 130310A in the first time bin, found together with a thermal component compared with that of GRB 110721A, is higher than the maximum temperature allowed by the non-saturated dissipative photosphere model, meaning that the Band component comes from an optically-thin region far above the photosphere. Besides, the hard-to-soft E_p evolution of GRB 130310A poses a challenge to the photosphere model. Although the internal shock and the ICMART are supposed to interpret the hard-to-soft E_p evolution in GRBs, the low σ internal shock model with typical value is lower than ~ 1 MeV, which is also hard for the high energy E_p of GRB 130310A to explain. The calculation of σ_{15} confirms that $r_0 \sim 10^9$ cm is essential to allow $(1 + \sigma_{15})>1$. However, the value of $(1 + \sigma_{15})$ is $\simeq 1$ in the zone z around 3 for $r_0 \sim 10^9$ cm. It suggests that the possibility of the origin from ICMART is not ruled out, but the value is very low. Seemingly, the photosphere-internal shock can interpret the high peak energy, which requires the electron Lorentz factor $\gamma_e \sim 60$ and $\epsilon_e \sim 0.06$. Together with GRB 110721A, it also suggests that, at least for some bursts, the Band component must invoke a non-thermal origin in the optically thin region of a GRB outflow.

It is worth noting that there is no observed redshift for GRB 130310A. The calculation for parameters of GRB 130310A (e.g., σ_0, σ_{15}, η, $r_{\rm ph}$, $\Gamma_{\rm ph}$, $\sigma_{\rm ph}$ and the value of E_p predicted in GRB theory models) relies on r_0 and z. Thus, we presume a series of values for the redshift $z \sim 0.1 \sim 8$, which enable us to investigate the high peak energy E_p of GRB 130310A in the first time bin.

Acknowledgements We thank the anonymous referee for suggestions that improved this paper. We thank

Prof. Bing Zhang for helpful suggestions. This work is supported by the National Natural Science Foundation of China (Grant Nos. 11673006, U1938201, 11533003), the Guangxi Science Foundation (Grant Nos. 2016GXNSFFA380006, 2017GXNSFBA198206, 2017AD22006, 2018GXNSFGA281007), the One-Hundred-Talents Program of Guangxi colleges, and High level innovation team and outstanding scholar program in Guangxi colleges. We also acknowledge the use of public data from the *Fermi* data archives.

References

Abbott, B. P., et al. 2017, ApJL, 848, L13
Abdo, A. A., Ackermann, M., Ajello, M., et al. 2009, ApJL, 706, L138
Akaike, H. 1974, IEEE Transactions on Automatic Control, 19, 716
Amati, L., Frontera, F., Tavani, M., et al. 2002, A&A, 390, 81
Arimoto, M., Asano, K., Ohno, M., et al. 2016, ApJ, 833, 139
Axelsson, M., et al. 2012, ApJL, 757, L31
Band, D., Matteson, J., Ford, L., et al. 1993, ApJ, 413, 281
Bégué, D., & Pe'er, A. 2015, ApJ, 802, 134
Beloborodov, A. M. 2010, MNRAS, 407, 1033
Berger, E., et al. 2005, Natur, 438, 988
Bhattacharya, M., & Kumar, P. 2020, MNRAS, 491, 4656
Bosnjak, Z., Götz, D., Bouchet, L., et al. 2013, in Cambresy L., Martins F., Nuss E., Palacios A., eds, SF2A-2013: Proceedings of the Annual meeting of the French Society of Astronomy and Astrophysics The spectral catalogue of INTEGRAL gamma-ray bursts, 455
Bošnjak, Ž., Daigne, F., & Dubus, G. 2009, A&A, 498, 677
Burnham, K. P., & Anderson, D. R. 2002, Technometrics, 45, 181
Butler, N., Watson, A. M., Kutyrev, A., et al. 2013, GRB Coordinates Network, 14350, 1
Cucchiara, A., Cenko, S. B., & Perley D. 2013, GRB Coordinates Network, 14289, 1
Dai, Z., Daigne, F., & Mészáros P. 2017, SSRv, 212, 409
Daigne, F., Bošnjak, Ž., & Dubus, G. 2011, A&A, 526, A110
Daigne, F., & Mochkovitch, R. 1998, MNRAS, 296, 275
Daigne, F., & Mochkovitch, R. 2002, MNRAS, 336, 1271
Eichler, D., Livio, M., Piran, T., et al. 1989, Nature, 340, 126
Fan, Y.-Z., Wei, D.-M., Zhang, F.-W., et al. 2012, ApJL, 755, L6
Fruchter, A. S., et al. 2006, Nature, 441, 463
Gao, H., & Zhang, B. 2015, ApJ, 801, 103
Ghirlanda, G., Pescalli, A., & Ghisellini G. 2013, MNRAS, 432, 3237
Ghisellini, G., Ghirlanda, G., Nava, L., et al. 2007, ApJL, 658, L75
Ghisellini, G., Ghirlanda, G., & Tavecchio, F. 2007, MNRAS, 375, L36
Giannios, D. 2008a, A&A, 480, 305
Giannios, D. 2012, MNRAS, 422, 3092
Goldstein, A., et al. 2012, ApJS, 199, 19
Golenetskii, S., Aptekar, R., Frederiks, D., et al. 2013, GRB Coordinates Network, 14285, 1
Golenetskii, S., et al. 2013, GCN, 14284, 1
Gruber, D., et al. 2014, ApJS, 211, 12
Guiriec, S., et al. 2011, ApJL, 727, L33
Guiriec, S., Daigne, F., Hascoët, R., et al. 2013, ApJ, 770, 32
Guiriec, S., Vianello, G., & Ohno, M. 2013, GRB Coordinates Network, 14282, 1
Hakkila, J., & Preece, R. D. 2011, ApJ, 740, 104
Hascoët, R., Daigne, F., & Mochkovitch, R. 2013, A&A, 551, A124
Hou, S.-J., Zhang, B.-B., Meng, Y.-Z., et al. 2018, ApJ, 866, 13
Ioka, K. 2010, Progress of Theoretical Physics, 124, 667
Ito, H., Matsumoto, J., Nagataki, S., et al. 2019, Nature Communications, 10, 1504
Kass, R. E., & Raftery, A. E. 1995, Journal of the American Statistical Association, 90, 773
Kawano, T., et al. 2013, GCN, 14310, 1
Kobayashi, S., Piran, T., & Sari, R. 1997, ApJ, 490, 92
Kumar, P., & Zhang, B. 2015, Phys. Rep., 561, 1
Larsson, J., Racusin, J. L., & Burgess, J. M. 2015, ApJL, 800, L34
Lazzati, D., & Begelman, M. C. 2010, ApJ, 725, 1137
Lazzati, D., Morsony, B. J., & Begelman, M. C. 2010, ApJ, 717, 239
Lei, W.-H., Zhang, B., Wu, X.-F., et al. 2017, ApJ, 849, 47
Liddle, A. R. 2004, MNRAS, 351, L49
Liddle, A. R. 2007, MNRAS, 377, L74
Liu, L.-D., Zhang, B., Wang, L.-J., et al. 2018, ApJL, 868, L24
Lü, H.-J., Lü, J., Zhong, S.-Q., et al. 2017, ApJ, 849, 71
Lu, R.-J., Wei, J.-J., Liang, E.-W., et al. 2012, ApJ, 756, 112
Lundman, C., Pe'er, A., & Ryde, F. 2013, MNRAS, 428, 2430
MacFadyen, A. I., & Woosley, S. E. 1999, ApJ, 524, 262
Meegan, C., et al. 2009, ApJ, 702, 791
Melia, F., & Maier, R. S. 2013, MNRAS, 432, 2669
Meng, Y.-Z., Geng, J.-J., Zhang, B.-B., et al. 2018, ApJ, 860, 72
Mészáros, P., & Rees, M. J. 1997, ApJ, 476, 232
Mészáros, P., & Rees, M. J. 2000, ApJ, 530, 292
Metzger, B. D., Giannios, D., Thompson, T. A., et al. 2011, MNRAS, 413, 2031
Nakar, E., & Piran, T. 2017, ApJ, 834, 28
Narayan, R., Paczynski, B., & Piran, T. 1992, ApJL, 395, L83
Nava, L., Ghirlanda, G., et al. 2011, A&A, 530, A21
Paczynski, B. 1986, ApJL, 308, L43
Paczynski, B. 1991, AcA, 41, 257
Parsotan, T., López-Cámara, D., & Lazzati, D. 2018, ApJ, 869, 103
Pe'er, A. 2008, ApJ, 682, 463
Pe'er, A. 2015, Advances in Astronomy, 2015, 907321
Pe'er, A., Mészáros, P., & Rees, M. J. 2006, ApJ, 642, 995
Pe'er, A., & Ryde, F. 2011, ApJ, 732, 49
Pe'er, A., & Ryde, F. 2017, International Journal of Modern Physics D, 26, 1730018

Pe'er, A., Zhang, B.-B., Ryde, F., et al. 2012, MNRAS, 420, 468
Piro, L., Troja, E., Gendre, B., et al. 2014, ApJL, 790, L15
Preece, R., et al. 2014, Sci, 343, 51
Preece, R. D., Briggs, M. S., Mallozzi, R. S., et al. 1998, ApJL, 506, L23
Preece, R. D., Briggs, M. S., Mallozzi, R. S., et al. 2000, ApJS, 126, 19
Ramirez-Ruiz, E., Celotti, A., & Rees, M. J. 2002, MNRAS, 337, 1349
Rees, M. J., & Meszaros, P. 1994, ApJL, 430, L93
Rees, M. J., & Mészáros, P. 2005, ApJ, 628, 847
Ryde, F., et al. 2010, ApJL, 709, L172
Ryde, F., Yu, H.-F., Dereli-Bégué, H., et al. 2019, MNRAS, 484, 1912
Sari, R., Piran, T., & Narayan, R. 1998, ApJL, 497, L17
Sbarufatti, B., Burrows, D. N., & Evans, P. E. 2013, GRB Coordinates Network, 14316, 1
Tan, M. Y. J., & Biswas, R. 2012, MNRAS, 419, 3292
Tanvir, N. R., Chapman, R., Levan, A. J., & Priddey, R. S. 2005, Nature, 438, 991
Thompson, C. 1994, MNRAS, 270, 480
Toma, K., Wu, X.-F., & Mészáros, P. 2011, MNRAS, 415, 1663
Uhm, Z. L., & Zhang, B. 2014, Nature Physics, 10, 351
Veres, P., Zhang, B.-B., & Mészáros, P. 2012, ApJL, 761, L18
Vurm, I., Beloborodov, A. M., & Poutanen, J. 2011, ApJ, 738, 77
Wang, X.-G., Zhang, B., Liang, E.-W., et al. 2015, ApJS, 219, 9
Wei, J.-J., Wang, J.-S., Gao, H., & Wu, X.-F. 2016, ApJL, 818, L2
Wei, J.-J., Wu, X.-F., & Melia, F. 2013, ApJ, 772, 43
Woosley, S. E. 1993, ApJ, 405, 273
Xiong, S., & Chaplin, V. 2013, GRB Coordinates Network, 14283, 1
Zhang, B. 2006, Nature, 444, 1010
Zhang, B. 2011, Comptes Rendus Physique, 12, 206
Zhang, B. 2014, International Journal of Modern Physics D, 23, 1430002
Zhang, B. 2015, in Thirteenth Marcel Grossmann Meeting: On Recent Developments in Theoretical and Experimental General Relativity, Astrophysics and Relativistic Field Theories Gamma-Ray Burst Prompt Emission, 224
Zhang, B. 2018, The Physics of Gamma-Ray Bursts
Zhang, B., Lu, R.-J., Liang, E.-W., & Wu, X.-F. 2012, ApJL, 758, L34
Zhang, B., & Mészáros, P. 2002, ApJ, 581, 1236
Zhang, B., & Pe'er, A. 2009, ApJL, 700, L65
Zhang, B., & Yan, H. 2011, ApJ, 726, 90
Zhang, B.-B., et al. 2018, NatAs, 2, 69
Zhang, B.-B., Zhang, B., Liang, E.-W., et al. 2011, ApJ, 730, 141